Under-expanded jets and dispersion in high pressure CO_2 releases from a large-scale pipeline

Xiaolu Guo [a], Xingqing Yan [a], Jianliang Yu [a†], Yongchun Zhang [b], Shaoyun Chen [b], Haroun Mahgerefteh [c], Sergey Martynov [c], Alexander Collard [c], Christophe Proust [d]

[a] School of Chemical Machinery and Safety,
Dalian University of Technology, Dalian, 116024,China

[b] School of Chemical Engineering,
Dalian University of Technology, Dalian, 116024, China

[c] Department of Chemical Engineering,
University College London, London WC1E 7JE, UK

[d] INERIS, Parc Technologique ALATA,
Verneuil-en-Halatte BP 2, 60550, France

[†]Corresponding Author
School of Chemical Machinery and Safety
Dalian University of Technology
No 2 Ling Gong Road
Dalian, 116024,China
e-mail: yujianliang@dlut.edu.cn
Tel.: +86 411 84986281
Fax: +86 13998576027

1 **Under-expanded jets and dispersion in high pressure CO$_2$ releases from a large-scale**
2 **pipeline**
3

4 Xiaolu Guo [a], Xingqing Yan [a], Jianliang Yu [a†], Yongchun Zhang [b], Shaoyun Chen [b],
5 Haroun Mahgerefteh [c], Sergey Martynov [c], Alexander Collard [c], Christophe Proust [d]

6

7 **Abstract**

8 As deeply development of Carbon Capture and Storage (CCS) project and massive

9 application of long-distance CO$_2$ pipeline, the inevitable pipeline rupture and leakage will

10 cause the catastrophic accidents. Study of near-field source terms and dispersion behavior

11 after pipeline rupture is essential foundation of CO$_2$ pipeline risk assessment and provide the

12 effective technical support for the implementation of large-scale CCS projects in the future. A

13 258 m long instrumental pipeline (233 mm i.d., 20 mm thickness) was used in CO$_2$QUEST

14 project to investigate the under-expanded jets and dispersion characteristics of a pipeline,

15 modelling puncture/rupture of a high pressure CO$_2$ pipeline. Video cameras, thermocouples

16 and CO$_2$ concentration sensors were deployed to monitor the formation of the visible cloud,

17 the distribution of the temperatures and concentrations in the dispersion area during the

18 gaseous and dense CO$_2$ release through the three orifice diameters (15 mm, 50 mm and Full

19 Bore Rupture). The under-expanded jet flow and the formation of the dry ice particles in the

20 near-field were studied for gaseous and dense CO$_2$ release. The safety distances along the

21 release direction of 5% concentration for each of the three orifice diameters were determined

22 by the lower limit for adverse human effects.

23

24 *Keyword:* CO$_2$ release, Under-expanded jet, Dispersion, Large-scale pipeline.
25
26

1   **1   Introduction**

2   A Large amount of CO_2 emissions lead to a series of problems such as environmental

3   deterioration, frequent extreme weather and so on, which promote the development of various

4   CO_2 mitigation technology [1]. As the most potential mitigation technology in the future,

5   Carbon Capture Storage (CCS) can fundamentally solve the problem of carbon emissions

6   from electric power industry, etc [2]. The urgency of deploying carbon capture and storage

7   (CCS) only increases if we are to achieve the stabilisation goal of low-carbon to limit the rise

8   in global temperatures to 2 °C above pre-industrial levels [3]. Therefore, CCS is the

9   important strategic choice to reduce carbon emissions and to control the climate warming.

10   The development and commercialization of CCS require an infrastructure for transportation

11   of the captured CO_2 from the sources of emission to the storage sites. It is commonly

12   accepted that pipeline transportation of CO_2 is considered as the safest and most efficient

13   transportation option [4]. The hazards associated with CO_2 pipelines are quite different

14   compared to those posed by hydrocarbon pipelines. The ability of CO_2 to collect in low-lying

15   areas near the pipeline route, presents a significant hazard if leaks continue undetected [5,6].

16   At a concentration of 10%, an exposed individual would lapse into unconsciousness in 1 min.

17   Furthermore, if the concentration is 20% or more, the gas is instantaneously fatal [7]. Safety

18   distances in published risk assessments for underground high pressure CO_2 pipelines vary

19   from less than 1 m till 7.2 km [8]. This large variation in the safety distance is difficult to

20   provide effective support for the actual security needs.

21   In the event of pipeline rupture, a significant proportion of the inventory would be discharged

1 in the first few minutes. Due to the relatively high Joule Thomson expansion coefficient CO_2

2 upon expansion may reach temperatures as low as -70 ^{o}C, which can induce brittle fracture

3 [9]. The large cooling effect associated with CO_2 expansion will cause the formation of dry

4 ice in the near-field [10]. A highly under-expanded flow will occur within the jet that contains

5 a Mach disk orthogonal to the flow direction [11]. The solid CO_2 particles formed in the jet,

6 which will subsequently sublimate and a vapor cloud will be formed and dispersed in the

7 far-field. In the process of mixing the momentum of the jet diminishes and the dispersion will

8 continue as a vapor cloud dispersion [12].

9 Many experimental studies have been conducted to establish a clear understanding of the

10 hazards associated with the failure of CO_2 pipelines. As part of the CO_2PipeHaz project,

11 INERIS [13-15] built a 2 m3 vessel fitted with a 9 m long pipe with an inner diameter of

12 50 mm to measure temperatures and concentrations in the modelled region of the flow field

13 for the experimental studies of large-scale CO_2 releases. An important conclusion was

14 obtained that significant solids are generated within the near-field of dense phase releases,

15 despite the release itself containing no dry ice. Xie et al. [16,17] developed a 23m long

16 circulating pipeline with a 30 mm inner diameter to study the pipeline leakage process of

17 supercritical CO_2 in a vertical direction. A typical highly under-expanded jet flow structure

18 was observed in the supercritical CO_2 leakage, which weakened with the depressurization in

19 the leakage process. The typical structure disappeared with the increasing of leakage nozzle

20 size. DNV-GL [18] conducted an experimental investigation to study the discharge of liquid

21 CO_2 from a 0.5 m^3 pressurized vessel equipped with an actuator valve. The results showed

1 that the CO_2 concentrations near the orifice depend mainly on the jet shape rather than the

2 mass flow rate. The concentrations at 9 and 15 m from the release point tend to increase

3 continuously during the saturation phase regime and then to drop with the transition to vapor

4 outflow. Xing et al [19] used a series of scaling rules to scale field experiments of CO_2

5 dispersion for simulating CO_2 blowouts. Through the comparison with the k–ϵ model and the

6 statistical performance indicators, it was concluded that the scaling rules were demonstrated

7 useful for the accidental release field experiment.

8 Several experimental research programs have been performed at the Spadeadam Test Site in

9 Cumbria, UK. The COSHER JIP [20] performed a large scale pipeline rupture test using a

10 226.6 m long pipeline loop formed from 219.1 mm diameter steel pipe and fed from both

11 ends by a 148 m^3 reservoir of CO_2. The results showed that a visible cloud reached a

12 maximum height of about 60 m and a maximum distance from the rupture location about

13 400 m. The pseudo-steady CO_2 concentrations were reached at the upwind and downwind

14 locations in the near-field in low wind speed conditions, but not reached in the far-field.

15 Wareing et al. [21,22] studied the venting of dense phase and gas phase CO_2 through a single,

16 straight vertical vent pipe of constant diameter within the framework of the COOLTRANS

17 research programme. The near-field dispersing structures of such releases were predicted by a

18 mathematical model against this experimental data. Witlox et al. [23,24] presented that BP

19 and Shell experimental work from CO_2 PIPETRANS JIP included both high-pressure

20 steady-state and time-varying cold CO_2 releases and high-pressure time-varying supercritical

21 hot CO_2 releases. For all cases the solid carbon dioxide was found to sublime rapidly and no

1   fallout was predicted.

2   As part of the CO_2QUEST project [25,26], this paper carried out six large-scale experiments

3   using a 258 m long, 233 mm inner diameter pipeline to study highly under-expanded jets and

4   dispersion characteristics of gaseous and dense CO_2 during sudden release under three orifice

5   sizes (15 mm, 50 mm and Full Bore Rupture). The experimental studies provided a detailed

6   understanding of the hazards presented by CO_2 releases through experimentation, which

7   could be used to validate the outflow and dispersion models developed.

8   **2   Experiments**

9   2.1 Experimental setup

10   Fig. 1 shows the schematic representation of the CO_2 pipeline employed for conducting the

11   release experiments. The release experiments involved the measurement of the temperature

12   and CO_2 concentration profiles in the discharge area using a 257 m long single pipeline with

13   low temperature carbon steel of 16MnR and a 1 m long dual-disc blasting pipe with grade

14   304 stainless steel. The experimental pipeline had a 233 mm internal diameter and a 20 mm

15   wall thickness, while had a maximum pressure rating of 16 MPa. Many concrete column

16   foundations were built to support the pipeline at a height of 1.3 m above ground. CO_2 release

17   experiments with different diameter punctures would be conducted using flanges with three

18   orifice sizes (15 mm, 50 mm and Full Bore Rupture) at various ambient temperatures up to a

19   maximum temperature of 40 ℃. The external heating for the pipeline was completed by a

20   1200 m long heating tape with 50 kW wrapped around the pipeline and a 50 mm thick

21   thermal insulation layer.

1   The dual-disc blasting device was consisted of two rupture discs and two disc holders, a

2   solenoid valve and two pipe sections, which was designed to made the release device safe,

3   controllable and being capable of transient release for conducting rupture and puncture

4   experiments. In principle, disk rupture corresponding to release occurs by reducing the

5   pressure difference between the two rupture discs using Nitrogen. Rupture experiments

6   involve fastening a flange incorporating different diameter orifices at the pipe release end.

7   Impulse and recoil forces of the pipeline set-up resulting from the sudden release could be

8   huge in such a large-scale experiment, and could be dangerous to people and the pipeline.

9   Therefore, a reinforcing device was designed to prevent the movement of the pipeline. The

10   device consists of steel frames and anchor bolts anchored firmly to the concrete foundation.

11   This reinforcement device can resist an acting force of 400 kN.

12   The feed procedure for CO_2 will be carried out as follows: (1) Decide the amount and state of

13   CO_2 to be fed into the pipeline and transport the CO_2 to the field. (2) Purge the pipeline first

14   using gaseous CO_2 to eliminate water and other impurities as far as possible. (3) Feed liquid

15   CO_2 into the pipeline using a tank car with vapour-liquid CO_2 of 2.2 MPa and -10 $^{\circ}$C. (4)

16   Shut down all valves when the appropriate mass of CO_2 had been injected to the pipe. (5)

17   Open the heating system to heat the main pipeline. (6) Isolate the experimental field when the

18   temperature and the pressure of the pipeline reached to the experimental conditions. (7)

19   Initiate the experiment through the dual-disc blasting device. (8) Record the measurement

20   data through data-acquisition systems during the release. (9) Clear up the experimental field

21   after the release.

1 2.2 Pipeline instrumentation

2 From the top of the view, the testing point locations were shown in Fig. 2. Three rows and

3 sixteen columns were set in the dispersion region. The distances from the orifice for each row

4 and column were labelled on the axial and the transversal direction. Thermocouples and CO_2

5 concentration sensors were both arranged on vertical tubes at the same height as the pipeline,

6 as shown in Fig. 3. The thermocouple was T-type with the uncertainty of ±1°C and the

7 measure range was -200 °C- 400 °C. The response times of the thermocouples was 100 ms.

8 The CO_2 concentration sensor was a COZIR-W type manufactured by Gas Sensing Solution

9 Ltd (GSS). The measure range was 0–100%, and the accuracy was ±3%. The response time

10 was 4 s.

11 Two data acquisition systems ran simultaneously in a computer, one was NI cRIO-9025

12 system which was used to sample the thermocouples, the other one was RS485

13 communication system which was used to sample the CO_2 concentration sensors. The NI

14 cRIO-9025 system consisted of one 9025, one 9144 chasses and two thermocouple input

15 modules of NI 9213. The RS485 communication bus adopted a twist-pair with RVVSP

16 2×2×0.5 mm^2 and a master-slave half duplex mode. The data-acquisition code was

17 programmed using LabVIEW software from the NI company.

18 A weather station was established to record the ambient temperature, ambient pressure,

19 ambient humidity, and wind speed and direction. The ambient pressure were measured using

20 QA-1 air pressure sensors with an accuracy of ±0.03 and a range of 55 kPa to 106 kPa. The

21 ambient temperature and humidity were measured using PTS-S environment monitoring

1   sensor with a uncertainty of ±0.1 ^{o}C and ±0.2, and a range of -50 ^{o}C to 80 ^{o}C and 0 to 100%.

2   The wind speed and direction were measured using EC-A1 ultrasonic wind sensor with an

3   accuracy of ±0.01 m/s and ±1°, and a range of 0 to 60 m/s and 0 to 360°. Several digital HD

4   video cameras and the Phantom 2 Vision aerial equipment were used to record the visible

5   cloud development during sudden release.

6   2.3 Experiments conducted

7   Six groups of CO_2 release experiments were performed to investigate dispersion behavior

8   during the release of gaseous and dense CO_2 from a pipeline with three orifice diameters

9   (15 mm, 50 mm and Full Bore Rupture). The purity of the CO_2 was 99.9%. The initial and

10   environmental conditions of six tests are presented in Table 1. For tests 1 and 4, the ambient

11   pressure and temperature, the wind speed and direction fluctuated violently as result of a long

12   depressurization time and the unstable atmospheric conditions. Other tests had a relative

13   stability of initial conditions.

14   **3   Experimental results**

15   3.1 Gas phase tests

16   3.1.1 Visible cloud development

17   For tests 1, 2 and 3 the total depressurization times for each experiment were 1946 s, 159 s

18   and 15 s respectively. According to the observation of the visible cloud in the experiments,

19   the development of visible cloud could be divided into the rapid expansion stage (I), the

20   metastable stage (II) and slow attenuation stage (III). For tests 1, 2 and 3, the duration times

21   of the initiation and stabilization stage were 2.5 s, 1 s and 0.6 s respectively, the duration

1   times of the metastable stage were 50 s, 4 s and 0.2 s respectively, the duration times of the

2   slow attenuation stage were 1894s, 154 s and 14.5 s respectively.

3   Fig. 4, 5 and 6 show the developments of the visible cloud for tests 1, 2 and 3. Due to the

4   Joule-Thomson cooling the temperature sharply dropped below the triple point near the

5   orifice and hence a white visible potential core could clearly be seen in the highly

6   under-expanded jet flow structure as a result of the formation of solid phase. For tests 1 and

7   2, the length of the visible cloud in the rapid expansion stage was fully developed at around

8   2.5 s and 1 s after the rupture respectively, remianed relatively stable within 50 s and 4 s in

9   the metastable stage respectively, and then turned into a slowly decaying while the expansion

10   angle of the jet flow decreased in the slow attenuation stage. The white visible cloud

11   disappeared in the forefront of the jet flow, indicating that the dry ice partcles gradually had

12   sublimated during diffusion.

13   For test 2. Jet boundary in near-field kept going in a straight line, which divergent angle

14   changed little in the whole process, circa 11°. Inside the jet dispersion, an extremely low

15   temperature led to a phase change of CO_2 from gas phase to solid phase. In the metastable

16   stage the spatial scale of the visible cloud remained unchanged and the length and the

17   maximum expansible radius of the visible cloud were circa 10 m and 1.5m respectively. At

18   the moment of 45 s and 60 s, the intercepting shock and the Mach disc could be clearly

19   observed in the jet flow.

20   For test 3. Jet velocities are indicated on the figure for the first 0.8 s. In the rapid expansion

21   stage the visible white cloud entraining the dry ice particles and condensed water rapidly

1   expanded and the expanding jet velocity gradually decreased. The visible cloud presented a

2   mushroom shape and reached a maximum distance of 40 m from the orifice. In the slow

3   attenuation stage the white visible cloud and the mixture of gaseous CO_2, air and raised dust

4   started to separate. When the limit of the former decayed to zero, the later continued to spread

5   relying on momentum, wind and body forces. For FBR test, because the dry ice particles

6   were spread farther away the considerable diffusion velocity and diffusion range of this test

7   could be observed. The divergent angle of jet boundary was circa 18° in test 3.

8

9   3.1.2 Temperature distribution

10   Fig.7 shows the temperature evolution along the axial line of the discharge area in tests 1, 2

11   and 3. After rupture, the ambient temperature in the far-field dropped as result of the

12   expansion of the escaping gas and the sublimation of the dry ice particles. The temperature

13   evolutions along the release direction gradually rose due to the reduction of the expanding

14   velocity and the fraction of dry ice along the axial direction. When the release ended, the

15   temperature of CO_2 gradually increased to the ambient condition along with time as the

16   continuous mixing of CO_2 mixture and air. For test 1, the temperature distribution range in

17   the dispersion region was small and fluctuated because of the small orifice release and the

18   unstable atmospheric environment. For test 2, the temperature contour lines with time quickly

19   extended along the axial direction and reached the maximum values at 15 s and then slowly

20   fell back. For test 3, the extending time and the down time of the temperature contour lines

21   were similar as result of the violent mixing of the escaping gas and air and the extremely

1 unstable atmosphere in the full bore release. The maximum temperature drop ampitudes of

2 the three experiments at distance of 4 m from the orifice were 4.2 °C, 5.5 °C and 17.6 °C

3 respectively and appeared at the time of 35 s, 15 s and 7 s respectively. The point in time of

4 the lowest temperatures became shorter and the maximum temperature drop ampitudes

5 became bigger with the increase of the orifice diameter due to the more violent mixing of the

6 escaping gas and air from a bigger hole release.

7 Fig. 8 shows the lowest temperature distribution in the discharge area of tests 1, 2 and 3. The

8 y direction is along the jet axis and x direction is horizontal distance. Obviously, the

9 temperature of the escaping gas increased along the x direction and the y direction in the

10 discharge area. The lengths of the temperature contour lines along the x direction were much

11 longer than that along the y direction than that along the y direction, while the temperature

12 gradients along the x direction were much lower. For 23 ^{o}C and 24 ^{o}C in test 1, 23 ^{o}C, 24 ^{o}C

13 and 25 ^{o}C in test 2, 10 ^{o}C, 13 ^{o}C and 16 ^{o}C in test 3, the length ratio between the temperature

14 contour lines along the y direction and the x direction were 16.1, 12.9, 33.5, 29.6, 21.3, 58.3,

15 30.4 and 24.1 respectively. This suggested that the temperature contour lines along the y

16 direction were much larger than that along the x direction, which was due to the greater

17 expanding velocities along the release direction. The length ratio between the temperature

18 contour lines along the x direction and the y direction became larger with the increase of the

19 orifice diameter. This was mainly because the jet velocities and distribution range became

20 greater with with the increase of the orifice diameter. For tests 1, 2 and 3, the length and

1   width of the low-temperature zone were predicted to 13 m and 2.5 m, 16 m and 2.2 m, 20 m

2   and 2.5 m in three tests respectively.

3

4   3.1.3 CO_2 concentration dispersion

5   Fig. 9 shows that the concentration development along the axial direction in tests 1, 2 and 3.

6   The acute health effects of high concentrations of inhaled CO_2 are influenced by two factors,

7   the concentration in the air and the duration of exposure. In concentrations of approximately

8   5% (50,000 ppm) within a few minutes the gas will cause headache, dizziness, increased

9   blood pressure, uncomfortable breathing and so on. Consequently, the threshold value of 5%

10   concentration is assumed to be the lower limit for adverse human effects [27].

11   For tests 1, 2 and 3, the contour of CO_2 concentration extended to the farthest point and

12   stayed in the metastable state. The closer distance from the orifice, the longer the duration

13   time would be in the area of 5% concentration. The start time of the contour of low CO_2

14   concentration was earlier than that of high CO_2 concentration, which was due to the response

15   lag of CO_2 concentration sensor as a result of high-velocity gas. But the response lag had a

16   little influence on the assessment of the dangerous concentration distances. For test 1, the

17   contour of CO_2 concentration extended to the farthest point at the distance of 9.2 m from the

18   release orifice, so the safety distance along the release direction in test 1 should be less than

19   10 m. For test 2, At the end of the release (159 s), CO_2 concentrations within the

20   measurement area stayed above 3% concentration, which decreased below 1% concentration

21   until 207 s after the rupture. The safety distance along the release direction in test 2 should be

at least 12 m. For test 3, the contour of 5% CO_2 concentration quickly extended to the farthest

point at 13 s. CO_2 concentrations at the distance of 5 m from the release orifice reached

30.1% at the end of the release (15 s), and reached the maximum value at 27 s, which stayed

above 5% concentration until 150 s after the rupture. This phenomenon was caused by the

sublimation of the dry ice particles in the discharge area. The safety distance in test 3 should

be at least 25 m. It was obvious that the larger discharge diameter brought a greater amount

of discharged CO_2 into the dispersion region over the same time interval.

3.2 Dense phase tests

3.2.1 Visible cloud development

For tests 4, 5 and 6 the total depressurization time of each experiment were 7300 s, 482 s and

40 s respectively. For tests 4, 5 and 6, the duration times of the rapid expansion stage were

9 s, 6 s and 5 s respectively, the duration times of the metastable stage were 441 s, 19 s and

1 s respectively, the duration times of the slow attenuation stage were 5850 s, 457 s and 35 s

respectively. Compared with the gas phase tests, the duration of each stage became longer.

Fig. 10, 11 and 12 show the developments of the visible clouds for tests 4, 5 and 6. At 0.5 s,

3 s and 6 s of test 4, the length and height of the visible cloud reached circa 11 m and 2.5 m,

25 m and 6 m, 36 m and 7 m respectievly, and the expanding velocity circa 11 m/s, 5 m/s and

4 m/s respectievly. This suggested that the length and height of the visible cloud became

larger gradully, and the expanding velocity became smaller gradully. For tests 5 and 6, the

length, width and height of the visible cloud reached circa 12 m, 3 m and 3 m, 22 m, 14 m

and 11 m at 0.5 s, and the expanding velocity circa 22 m/s and 32 m/s at 0.5 s respectievly.

The indicated that the sizes of the visible cloud and the expanding velocity became larger at

the same time as the orifice size increased. For test 4, the length, width and height of the

visible cloud reached the maximum value at 9 s. For tests 5 and 6, the maximum length and

width of the cloud were circa 80 m and 30 m at 6 s, 150 m and 70 m at 5 s respectively, but

the heigh of the cloud reached the maximum value circa 12 m at 2 s and 16 m at 1 s

respectively. This shown that the length and width of the cloud were still rising when the

heigh of the cloud reached the maximum. The influence of the orifice size on the height was

quite obvious because the angle of reflection of the high-velocity jet flow at the ground was

greater as the orifice size increased. However the width of the cloud was greater than the

heigh of that due to the effect of the dry ice and heavy gas.

For three dense phase tests, the divergent angle of the jet boundary reached the maximum

value at the moment of the rupture and decreased gradully in the whole process. In the rapid

expansion stage the jet flow expanded rapidly and the leading edge of the jet presented a arc

surface, while the straight length of jet boundary in near-field increased quickly. In the

metastable stage, the forefront of the cloud presented a fan-shaped form and the length of the

jet boundary and the visible cloud remained unchanged nearly. The heavy gas effect started

prompting the free diffusion of CO_2 in the low-lying areas. In the slow attenuation stage,

because of the loss of the expanding velocity the visible cloud diffused mainly depending on

the residual momentum. The sizes of the visible cloud began to decay and the attenuation

velocity changed from fast to slow. The maximum length and divergent angle of jet boundary

1   were greater as the orifice size increased. Compared to the gas phsae tests, the visible cloud

2   produced in the dense phase tests had a much wider dispersion range and a greater formation

3   amount of the dry ice particles and the condening water. The condensation of water saturated

4   in the ambient air was relevant to the environmental humidity and the pipeline pressure.

5   3.2.2 Temperature distribution

6   Fig. 13 shows the temperature evolution along the axial line of the discharge area in tests 5

7   and 6. For test 4 the temperatures in the dispersion area were missing as the result of the

8   shedding of an aviation connector used for data acquisition. For test 5, the temperature

9   contour lines quickly extended along the axial direction with time and reached the farthest

10   distance at 13 s, while the temperature drop amplitude at the location of 5 m reached the

11   maximum value of 31 ^{o}C, which was larger than that in test 2. For test 6, the temperature

12   drop amplitude reached 24 ^{o}C at 3 s, which was larger than that at the same time for test 2.

13   The temperature drop amplitude reached the maximum value of 102 ^{o}C at 17 s. This time was

14   longer than 3 s in test 3 due to the continuous sublimation of a number of dry ice particles in

15   test 6. The results indicated that there was a similar characteristic of the temperature

16   evolution along the release direction between the dense and the gas phase tests. However, it's

17   extremely obvious that the low-temperature areas in the dense phase tests were much greater

18   than that in the gas phase tests under the same orifice size.

19   Fig. 14 shows the lowest temperature distribution in the discharge area of tests 5 and 6. The y

20   direction is along the jet axis and x direction is horizontal distance. The overall temperature

21   distribution trend was that the temperature gradients along the x direction were much lower

1 than along the y direction, while the lengths of the temperature contour lines along the x

2 direction were much longer than those along the y direction. For 0 $^{\circ}$C, 3 $^{\circ}$C, 6 $^{\circ}$C and 9 $^{\circ}$C in

3 test 5, the length ratio between the temperature contour lines along the y direction and the x

4 direction were close to 10.1. This indicated that the temperature distribution shifted to the

5 right due to the effect of the southeast wind. For -40 $^{\circ}$C, -30 $^{\circ}$C, -20 $^{\circ}$C and -10 $^{\circ}$C in test 6,

6 the length ratio between the temperature contour lines along the y direction and the x

7 direction were 96.6, 45.6, 32.7 and 27.1 respectively. This shown that the diffusioin velocity

8 in the FBR release of dense phase tests was extremely fast and the temperature distribution

9 could be considered axisymmetric. According to the contour extending trend in tests 5 and 6,

10 it's predicted that the macimum length and width of the low-temperature zone were 16 m and

11 3 m, 30 m and 5 m in both tests respectively.

12 3.2.3 CO_2 concentration dispersion

13 Fig. 15 shows the evolution of CO_2 concentration along the axial direction in tests 4, 5 and 6.

14 For test 4, CO_2 concentrations at a distance of 5 m from the release orifice at 15 s reached 5%

15 v/v concentration and remained this quasi steady state level until 3200 s. The concentrations

16 at the farthest distance of 19.2 m from the orifice at 263 s reached 5 %, so the safety distance

17 along the release direction in test 4 should be circa 20 m. For test 5, the concentration contour

18 lines fluctuated violently at some time points due to the influence of the southeast wind. CO_2

19 concentrations inside the measurement area at 6 s reached 5% v/v concentration and at a

20 distance of 12 m from the release orifice had remained above 5% at the end of the release

21 (482 s). The safety distance along the release direction in test 5 should be circa 60 m. For test

1 6, the CO_2 concentration contours began to stretch at 6 s and extended to their farthest point

2 at 15 s. At the end of the release (40 s) CO_2 concentrations at a distance of 60 m from the

3 release orifice had remained above 5% v/v concentration as a result of the continual

4 sublimation of the dry ice particles. The time of the maximum concentration (61% v/v) 20 m

5 from the orifice was earlier than the time of the maximum concentration (100% v/v) 5 m

6 from the orifice. This suggested that because of the effect of the dry ice sublimation and the

7 response time of the sensors the duration time of the maximum value were longer as the

8 distance from the orifice decreased. The safety distance along the release direction in test 6

9 reached circa 160 m.

10 **4 Discussions**

11 This paper studied the highly under-expanded jets and dispersion characteristics of gaseous

12 and dense CO_2 during sudden release from a large-scale pipeline. Such a large capacity

13 pipeline was essential as it permitted the shock tube depressurization tests for long enough

14 duration to capture sufficient data for analysis. A great many sensors were used to monitor the

15 formation of the visible cloud, the distribution of the temperatures and concentrations in the

16 far-field. The research results of near-field source terms and dispersion behavior in this study

17 were necessary and of paramount importance for assessing safety distances and the impact of

18 CO_2 pipeline releases on the surrounding environment, which were rare, reliable and close to

19 the actual applications.

20 Depressurization of high pressure CO_2 following pipeline rupture or puncture, and

21 subsequent dispersion, will almost certainly involve the high-velocity jet flow and the

1   transition between different physical states. Because the pre-expansion to post-expansion

2   pressure ratio resulting from a release will initially be large, the sonic velocity will be reached

3   at the outlet of the pipe and the resulting free jet will be sonic. This leads to a highly under

4   expanded flow that contains a Mach disk, the precise form of which depends on the ratio of

5   the exit to the atmospheric pressure. For CO_2 releases, the temperature and pressure decrease

6   that accompanies the initial expansion will lead to the formations of dry ice particles and

7   condensing water vapor. Likewise, sublimation of the dry ice particles results in heat removal

8   from the gas phase and an associated temperature decrease. Formation of solid CO_2 will

9   affect the shape and properties of a CO_2 cloud in ways different to a gas/liquid cloud [28]. In

10   addition, Ground topography and physical objects as well as wind direction may have a

11   significant influence on the spread and movement of a CO_2 cloud. These extremely

12   complicated phenomena will be contained in the dispersion process of gaseous and dense

13   CO_2 during sudden release. The high pressure CO_2 dispersion theoretical/modelling involves

14   the appropriate source terms, the three-phase accurate equation of state in the near-field

15   prediction, the suitable species transport, the precise particle tracking techniques for

16   estimating the amount of solid CO_2, the effect of heat transfer between the ground and the

17   flowing fluid, the more accurate turbulence modeling [29-31]. Because all these processes

18   need to be included within any dispersion model, no mathematical model is currently capable

19   of predicting such complex releases.

20   Currently, we concentrate mainly on the experimental research and has a lack of theoretical

21   analysis. However this large-scale experimental results could be applied as important basic

data for CO_2 dispersion research and used to validate the outflow, near-field and far filed dispersion models. Experimental characterisation of the temperatures in the immediate region of a release will also be performed to enable estimation of the risk to piping, plant or structures from embrittlement due to low temperatures. For the design, construction and operation of new high pressure CO_2 pipelines through populated areas the safety distance along the release direction of 5% v/v concentration obtained from the experiments can be considered as applied reference. This is critically important when performing consequence failure analysis and significant hazard quantification for CO_2 pipelines. The more deeply experimental and theoretical studies were conducted on the dispersion behavior during sudden release under complicated situation in the future.

5 Conclusions

This article has presented the results of a large-scale experimental study of under-expanded jets and dispersion characteristics of gaseous and dense CO_2 following pipeline rupture using three orifice sizes (15 mm, 50 mm and Full Bore Rupture). According to the experimental study, some conclusions are demonstrated as follows:

(1) A highly under-expanded flow that contained a Mach disk would be developed near the orifice during the release of high pressure CO_2. A large of dry ice particles formed in the near-field dispersion due to the Joule-Thomson cooling, and then were brought into the far-field by jet flow. The dispersing cloud was made visible by the presence of the dispersed white dry ice particles and condensing water vapor. However no dry ice bank appeared on the ground surface in the tests due to the rapid sublimation of the solid CO_2 particles before

falling to the ground.

(2) After rupture, the ambient temperature in the far-field dropped as result of the expansion of the escaping gas and the sublimation of the dry ice particles. The temperature evolutions along the release direction gradually rose due to the reduction of the expanding velocity and the fraction of dry ice along the axial direction. As the orifice diameter increased under the same initial pressure and temperature the temperature drop amplitude and the dispersion distance of CO_2 in the discharge area increased and the safety distance of 5% v/v concentration became greater.

(3) Compared to the gas phsae tests, the visible cloud produced in the dense phase tests had a much wider dispersion range and a greater formation amount of the dry ice particles and condensing water vapor. The low-temperature areas and the safety distance in the dense phase tests were much greater than that in the gas phase tests. The heavy gas effect prompted a large number of CO_2 to accumulate in low-lying place when there is no wind.

1   **References**

2   [1]   Haszeldine RS. Carbon capture and storage: how green can black be? Nature 2009;

3   325:1647-1652.

4   [2]   Munkejord ST, Hammer M, Løvseth SW. Intergovernmental panel on climate change,

5   carbon capture & storage, ISBN 92-9169-119-4. Appl Energy 2016; 169:499–523.

6   [3]   IEA, Energy Technology Perspectives 2008, Paris: France, 2008.

7   [4]   Chong FK, Lawrence KK, Lim PP, Poon MCY, Foo DCY, Lam HL, Tan RR PP.

8   Planning of carbon capture storage deployment using process graph approach. Energy

9   2014; 76:641-651.

10   [5]   Iribarren D, Petrakopoulou F, Dufour J. Environmental and thermodynamic evaluation

11   of CO_2 capture, transport and storage with and without enhanced resource recovery.

12   Energy 2013; 50:477-85.

13   [6]   Duncan IJ, Wang H. Estimating the likelihood of pipeline failure in CO_2 transmission

14   pipelines: New insights on risks of carbon capture and storage. Int J Greenh Gas Con

15   2014; 21: 49-60.

16   [7]   Brown S, Beck J, Mahgerefteh H. Global sensitivity analysis of the impact of impurities

17   on CO_2 pipeline failure. Reliab Eng Syst Safe. 2013; 115: 43–54.

18   [8]   Molag M, Dam C. Modelling of accidental releases from a high pressure CO_2 pipelines.

19   Energy Procedia 2011; 4:2301-2307.

20   [9]   Botros KK, Hippert E Jr, Craidy P. Measuring decompression wave speed in CO_2

21   mixtures by a shock tube. Pipelines International 2013; 16:22-28.

[10] Mazzoldi A, Hill T, Colls JJ. CO_2 transportation for carbon capture and storage: Sublimation of carbon dioxide from a dry ice bank. Int J Greenh Gas Con 2008 2:210-218.

[11] Witlox HWM, Harper M, Oke A. Modelling of discharge and atmospheric dispersion for carbon dioxide releases. J Loss Prevent Proc 2009; 22:795-802.

[12] Witkowski A, Rusin A, Majkut M, Rulik S, Stolecka K. Comprehensive analysis of pipeline transportation systems for CO_2 sequestration. Energ Convers Manage 2013; 76: 665-673.

[13] Woolley RM, Fairweather M, Wareing CJ, Falle SAEG, Proust C, Hebrard J, Jamios D. Experimental measurement and Reynolds-averaged Navier–Stokes modelling of the near-field structure of multi-phase CO_2 jet releases. Int J Greenh Gas Con 2013; 18:139–149.

[14] Gant SE, Narasimhamurthy VD, Skjold T, Jamois D, Proust C. Evaluation of multi-phase atmospheric dispersion models for application to Carbon Capture and Storage. J Loss Prevent Proc 2014; 32:286-298.

[15] Woolley RM, Fairweather M, Wareing CJ, Falle SAEG, Mahgerefteh H, Martynov S, Brown S, Narasimhamurthy VD, Storvik IE, Sælen L, Skjold T, Economou IG, Tsangaris DM, Boulougouris GC, Diamantonis NI, Cusco L, Wardman M, Gant SE, Wilday J, Zhang YC, Chen SY, Proust C, Hebrard J and Jamois D. CO_2PipeHaz: quantitative hazard assessment for next generation CO_2 pipelines. Energy Procedia 2014, 63:2510–2529.

[16] Xie QY, Tu R, Jiang X, Li K, Zhou XJ. The leakage behavior of supercritical CO_2 flow in an experimental pipeline system. Appl Energy 2014; 130:574-580.

[17] Li K, Zhou XJ, Tu R, Xie QY, Jiang X. The flow and heat transfer characteristics of supercritical CO_2 leakage from a pipeline. Energy 2014; 71:665-672.

[18] Ahmad M, Osch MB, Buit L, Florisson O, Hulsbosch-Dam C, Spruijt M, Dacolio F. Study of the thermohydraulics of CO_2 discharge from a high pressure reservoir. Int J Greenh Gas Con 2013; 19:63-73.

[19] Xing J, Liu ZY, Huang P, Feng CG, Zhou Y, Sun RY, Wang SG. CFD validation of scaling rules for reduced-scale field releases of carbon dioxide. Appl Energy 2014; 115: 525-530.

[20] Ahmad M, Lowesmith B, Koeijer Gd, Nilsen S, Tonda H, Spinelli C, Cooper R, Clausen S, Mendes R, Florisson O. COSHER joint industry project: Large scale pipeline rupture tests to study CO_2 release and dispersion. Int J Greenh Gas Con 2015; 37:340–353.

[21] Wareing CJ, Fairweather M, Falle SAEG, Woolley RM. Validation of a model of gas and dense phase CO_2 jet releases for carbon capture and storage application. Int J Greenh Gas Con 2014; 20:254-271.

[22] Wen J, Heidari A, Xu BP, Jie HG. Dispersion of carbon dioxide from vertical vent and horizontal releases—A numerical study. J Process Mechanical Engineering 2013; 227:125-139.

[23] Witlox HWM, Harper M, Oke A, Stene J. Validation of discharge and atmospheric dispersion for unpressurised and pressurised carbon dioxide releases. Process Saf

1   Environ 2014; 92:3-16.

2   [24] Witlox HWM, Harper M, Oke A, Stene J. Phast validation of discharge and atmospheric

3   dispersion for pressurised carbon dioxide releases. J Loss Prevent Proc 2014;

4   30:243-255.

5   [25] Brown S, Martynov S, Mahgerefteh H, Fairweather M, Woolley RM, Wareing CJ, Falle

6   SAEG, Rutters H, Niemi A, Zhang YC, Chen SY, Besnebat J, Shah N, Dowell NM,

7   Proust C, Farret R, Economou IG, Tsangaris DT, Boulougouris GC, Wittenberghe JV.

8   CO_2QUEST: Techno-economic assessment of CO_2 quality effect on its storage and

9   transport. Energy Procedia 2014; 63:2622-2629.

10   [26] Guo XL, Yan XQ, Yu JL, Zhang YC, Chen SY, Mahgerefteh H, Martynov S, Collard A,

11   Proust C. Pressure response and phase transition in supercritical CO2 releases from a

12   large-scale pipeline. Appl Energy 2016; 178:189-197.

13   [27] Kruse H, Tekiela M. Calculating the consequences of a CO_2-pipeline rupture. Energy

14   Convers 1996; 37:1013-1018.

15   [28] Harper P, Wilday J, Bilio M. Assessment of the Major Hazard Potential of Carbon

16   Dioxide (CO_2). Health and Safety Executive 2011; 1-28.

17   [29] Zhou XJ, Li K, Tu R, Yi JX, Xie QY, Jiang X. A modelling study of the multiphase

18   leakage flow from pressurized CO_2 pipeline. J Hazard Mater 2016; 306:286-294.

19   [30] Wareing CJ, Woolley RM, Fairweather M, Falle SAEG. A composite equation of state

20   for the modeling of soniccarbon dioxide jets in carbon capture and storage scenarios.

21   AIChE J 2013; 59:3928-3942.

1   [31] Wareing CJ, Fairweather M, Falle SAEG, Woolley RM. Modelling punctures of buried

2   high-pressure dense phase CO_2 pipelines in CCS applications. Int J Greenh Gas Con

3   2014; 29:231-247.

4

5

1　　Table 1　Experimental conditions and environmental conditions

Number	Test1	Test2	Test3	Test4	Test5	Test6
Pressure (MPa)	4.05	4.0	3.6	9.2	9.1	9.1
Temperature (℃)	33.8	33.4	32.7	17.4	19.3	21.6
Orifice (mm)	15	50	FBR	15	50	FBR
Inventory (tons)	0.97	0.96	0.84	9.48	9.31	9.11
Ambient pressure (kPa)	99.6	99.7	99.5	99.9	99.6	99.8
Ambient temperature (^{o}C)	26.4~26.8	27.5	23.6	24.9~27.4	25.2	30.1
Humidity (%)	87.6~86.8	80.2	82.3	98.1~87.8	80.1	86.7
Wind speed (m/s)	0.6~1.8	1.6	0	0.7~2.4	2.3	1.0
Wind direction	120~168	108	0	238~289	149	36
Atmospheric stability	B	B	A	B	B	B

2

3

4

N

W ← → E

S

258 m

55° S

CO$_2$ tank car

Main pipeline

Disc A (P_A)   Disc B (P_B)

Main pipeline   Section I   Section II   Blank flange

CO$_2$(P_1)   N$_2$(P_2) P_a Release orifice

Solenoid valve

N$_2$ injection line

Dual-disc blasting device

Discharge area

Measuring points

Video camera
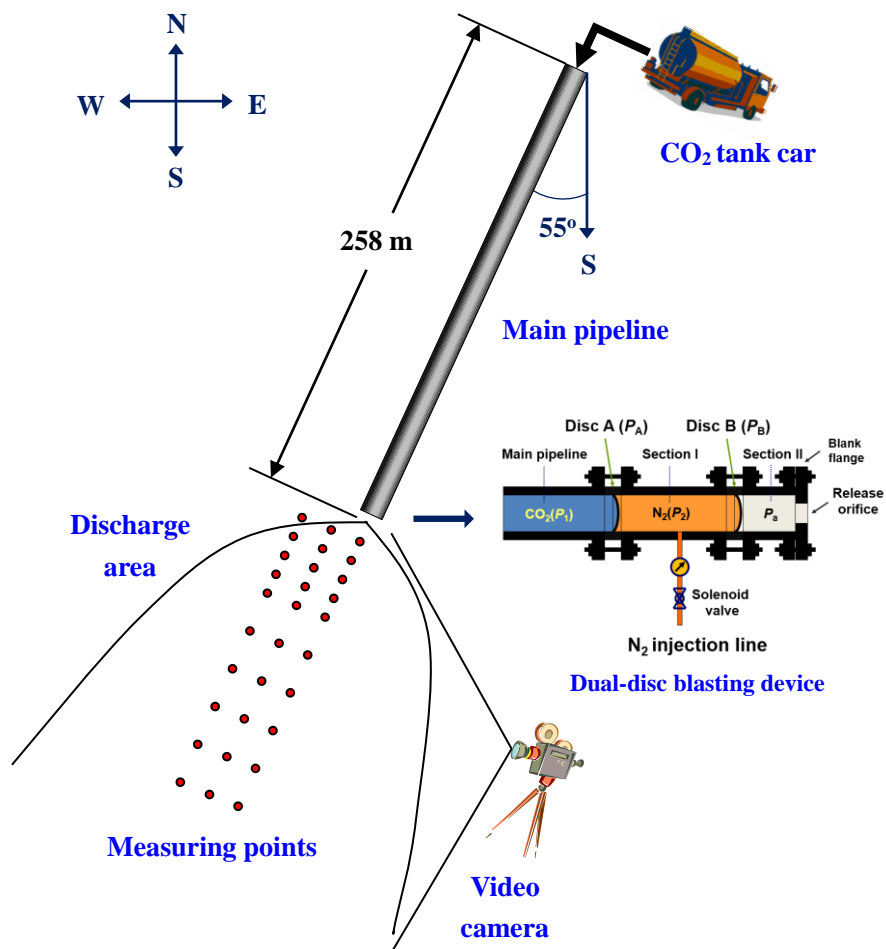
Fig. 1 Process flow.
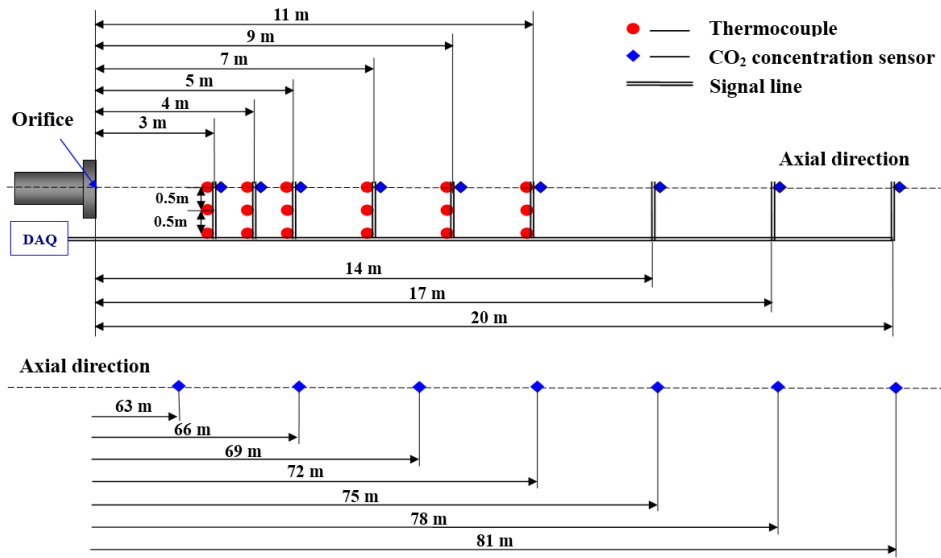
Fig. 2 Distribution of measurement points in discharge area.
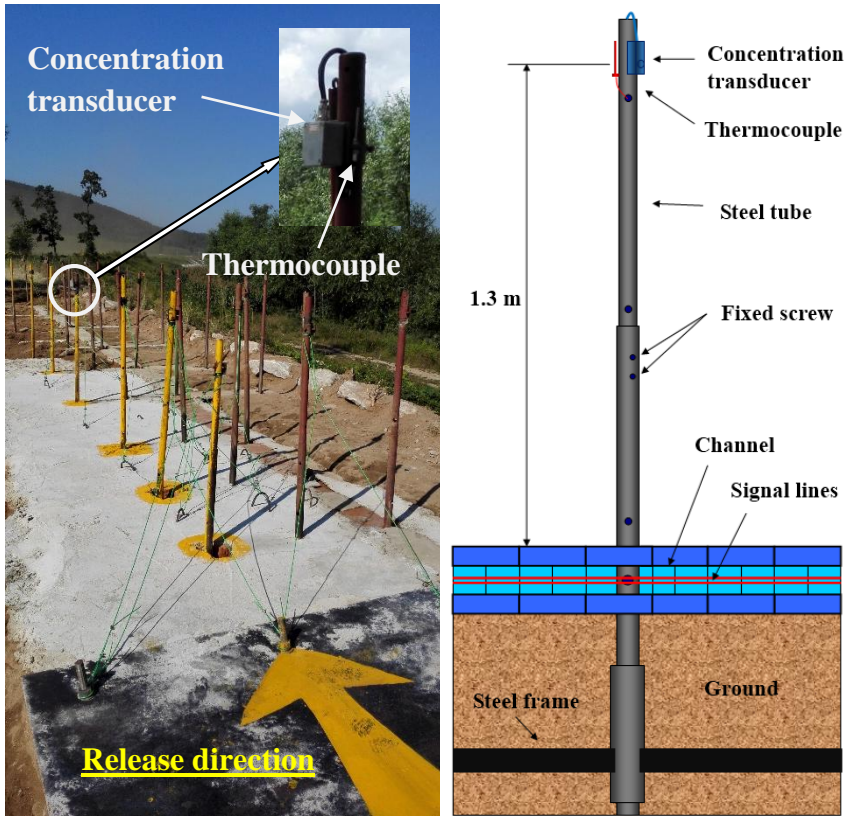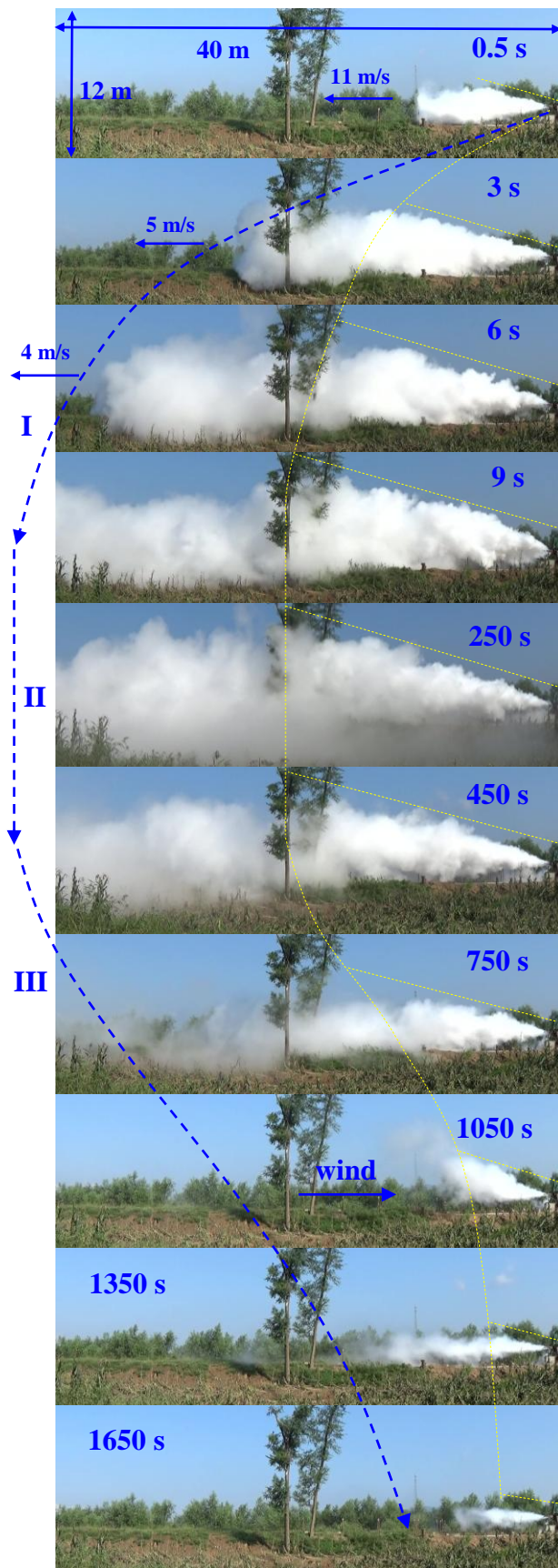
Fig. 3 CO2 concentration sensor and installation.
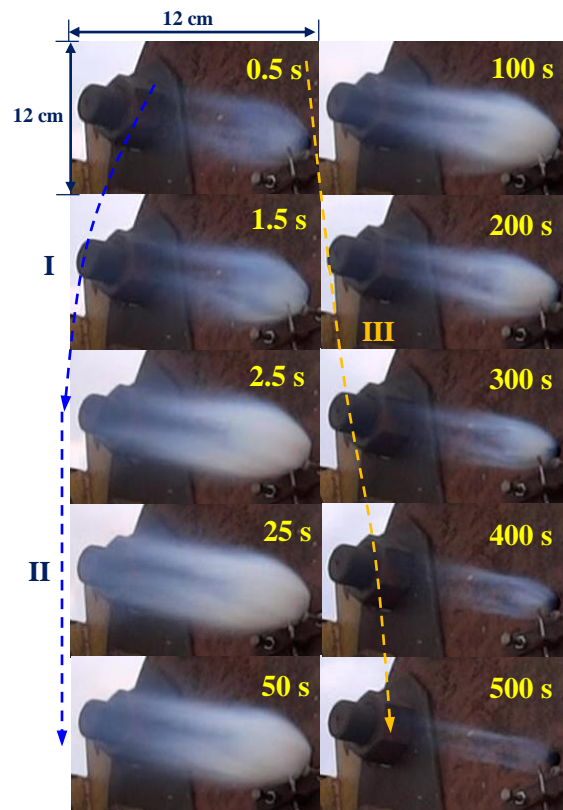
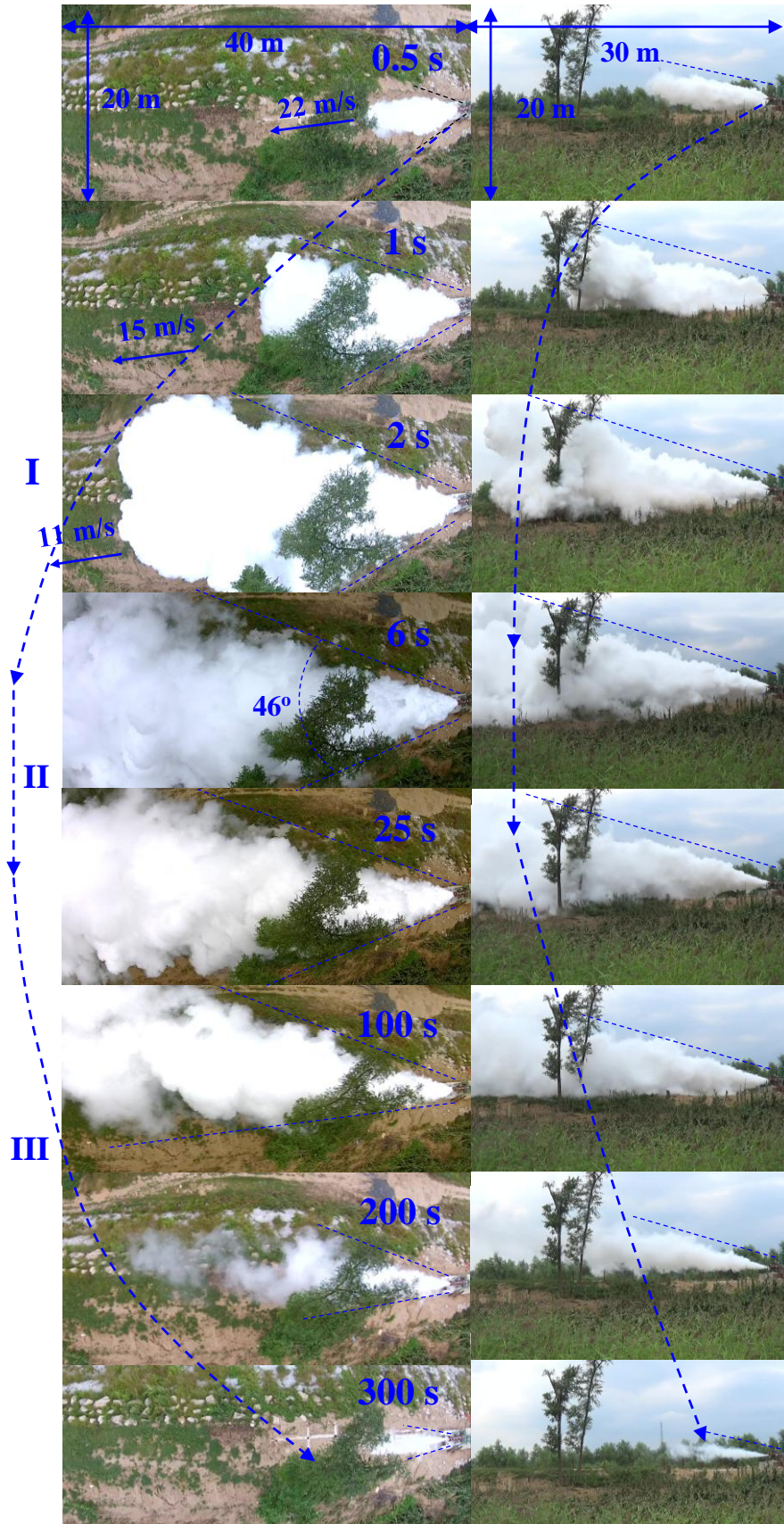Fig. 4 Visible cloud development of the gaseous CO_2 release experiments with 15 mm orifice.
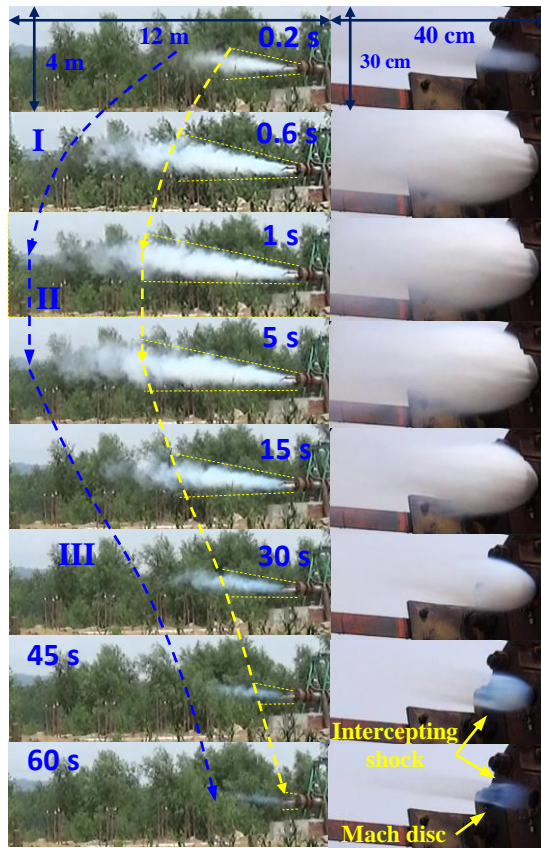
Fig. 5 Visible cloud development of the gaseous CO_2 release experiments with 50 mm orifice.
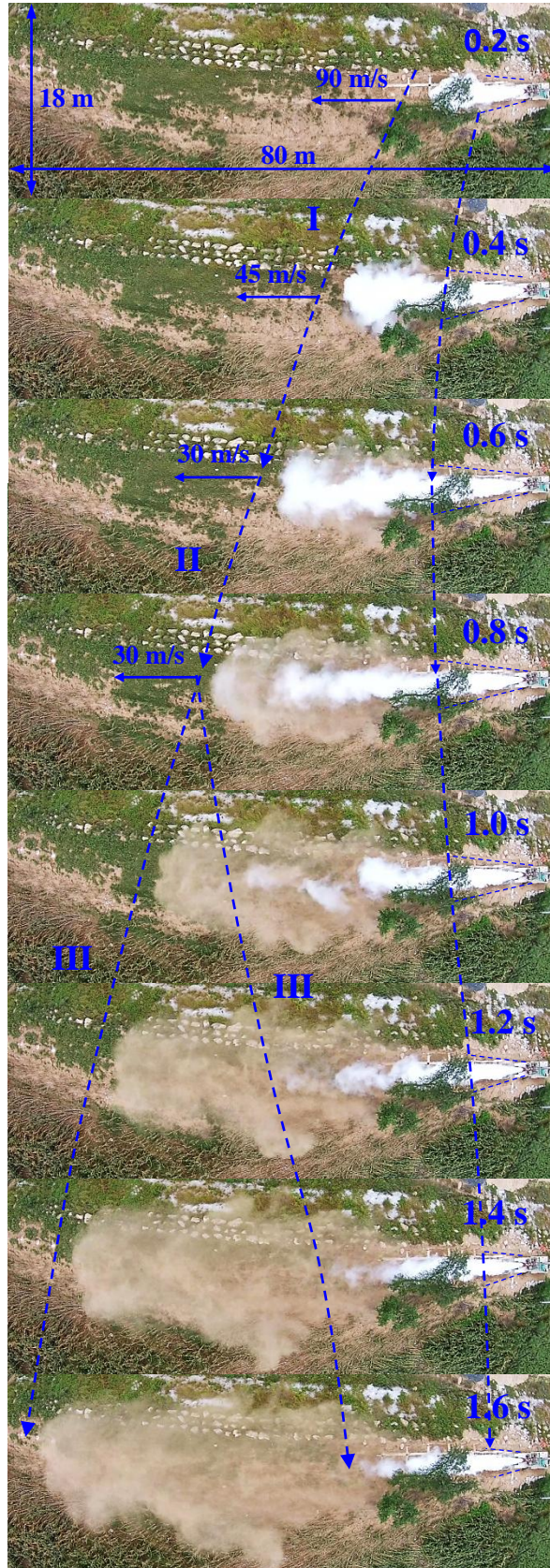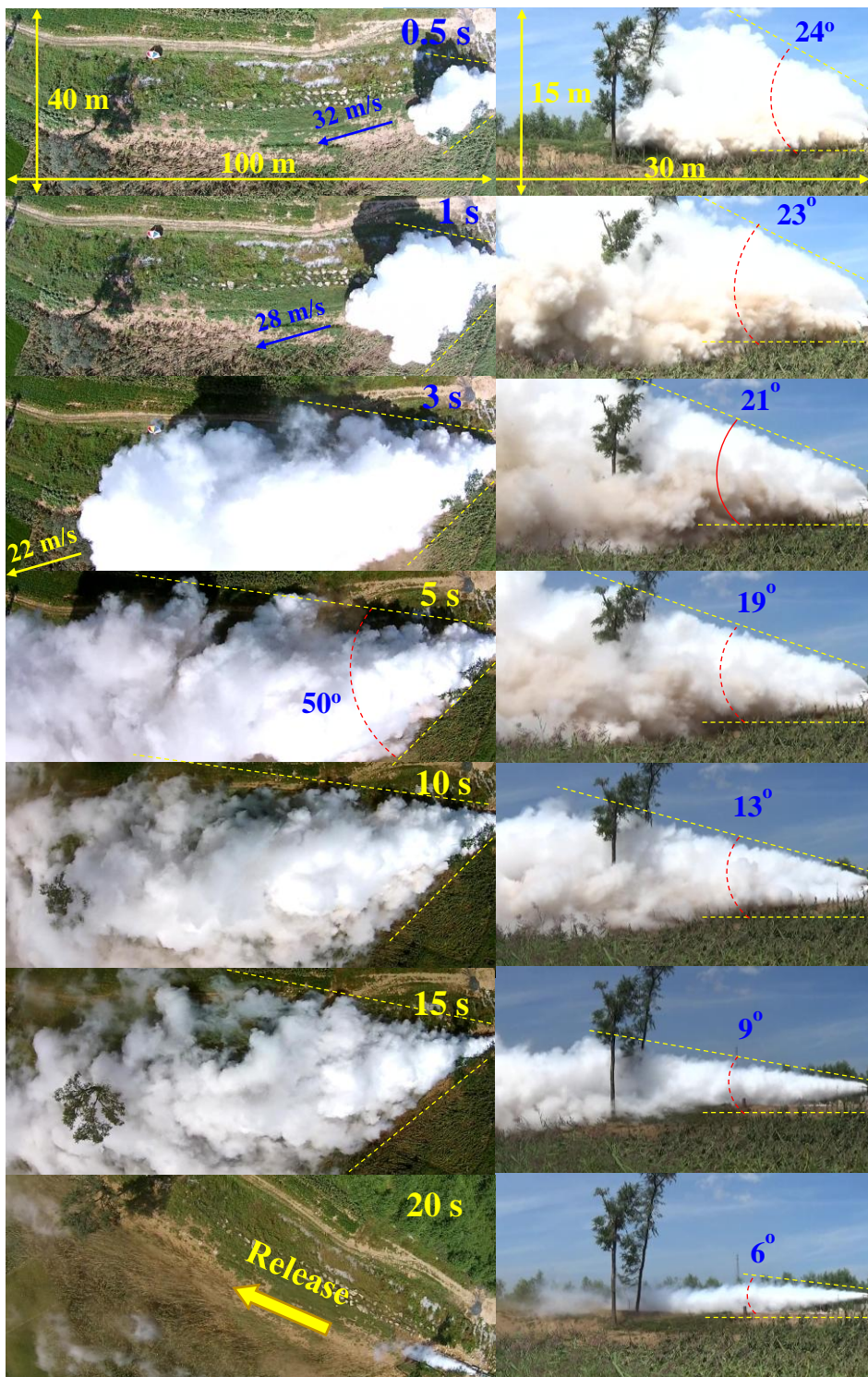
Fig. 6 Visible cloud development of the gaseous CO$_2$ release experiments with the full bore orifice.
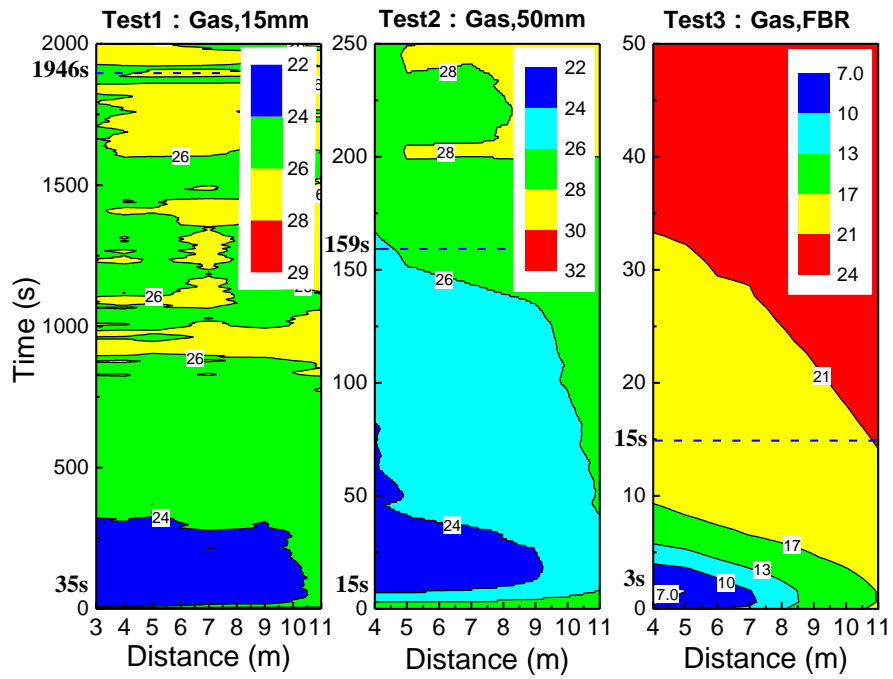
Fig. 7 Temperature evolutions along the centerline of the gaseous CO_2 release experiments with three different orifices (15 mm, 50 mm and FBR).
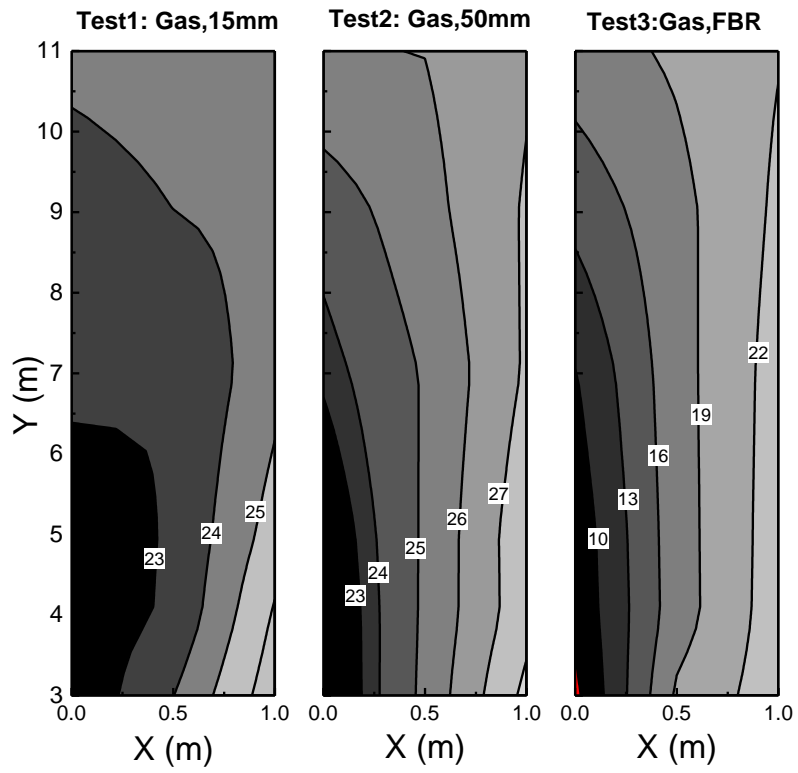
Fig. 8 Temperature distribution area of the gaseous CO_2 release experiments with three different orifices (15 mm, 50 mm and FBR).
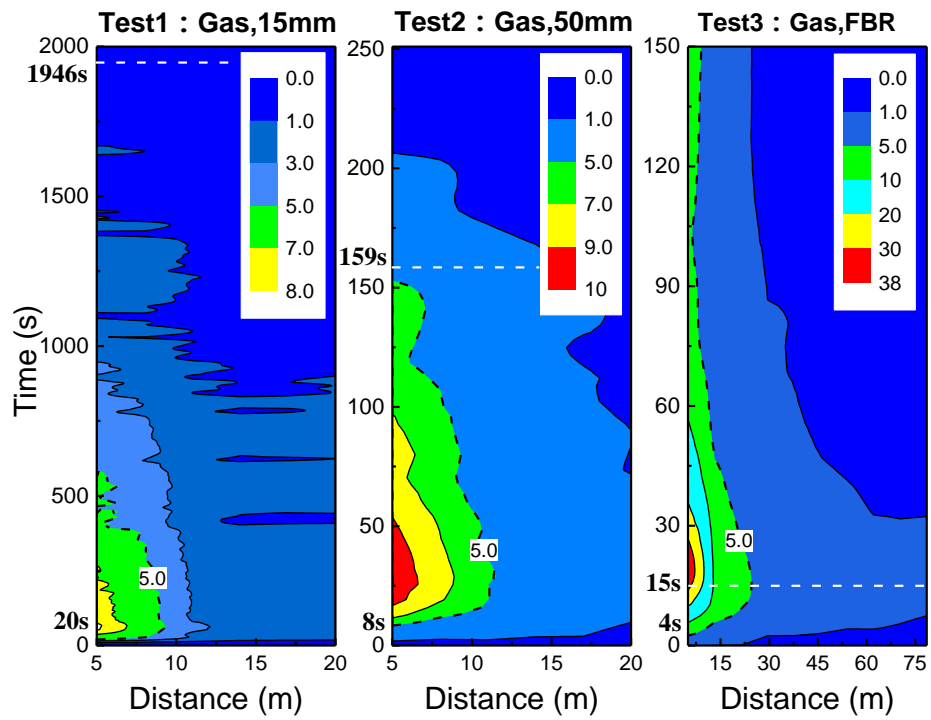
Fig. 9 CO$_2$ concentration development along the centerline of the gaseous CO$_2$ release experiments with three different orifices (15 mm, 50 mm and FBR).

Fig. 10 Visible cloud development of the dense CO_2 release experiments with 15 mm orifice.

Fig. 11 Visible cloud development of the dense CO_2 release experiments with 50 mm orifice.

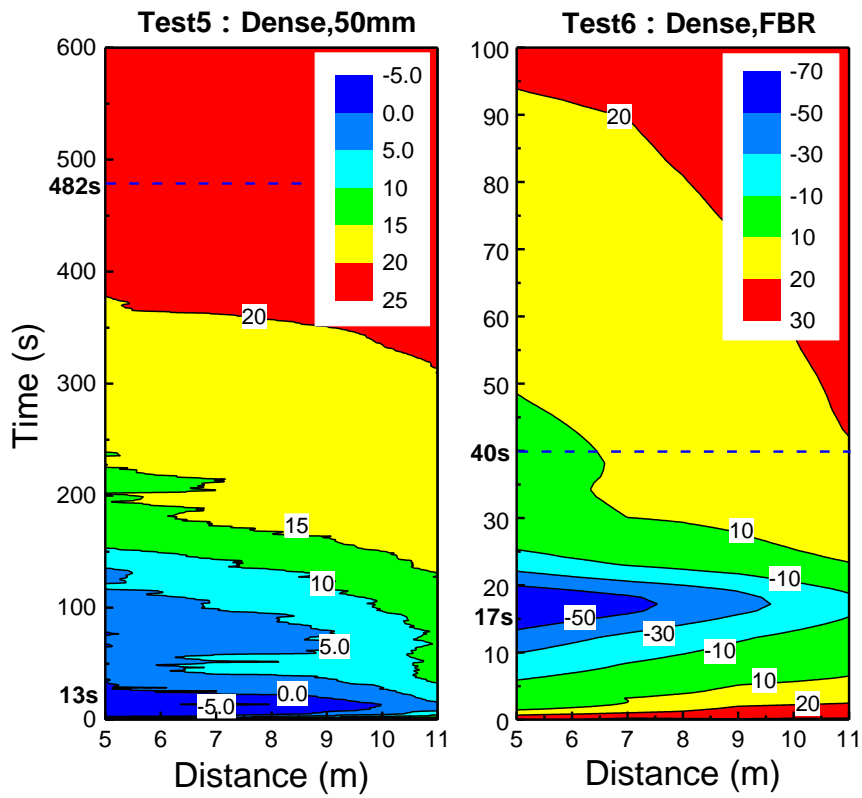Fig. 12 Visible cloud development of the dense CO_2 release experiments with the full bore orifice.

Fig. 13 Temperature evolutions along the centerline of the dense CO₂ release experiments with three different orifices (15 mm, 50 mm and FBR).
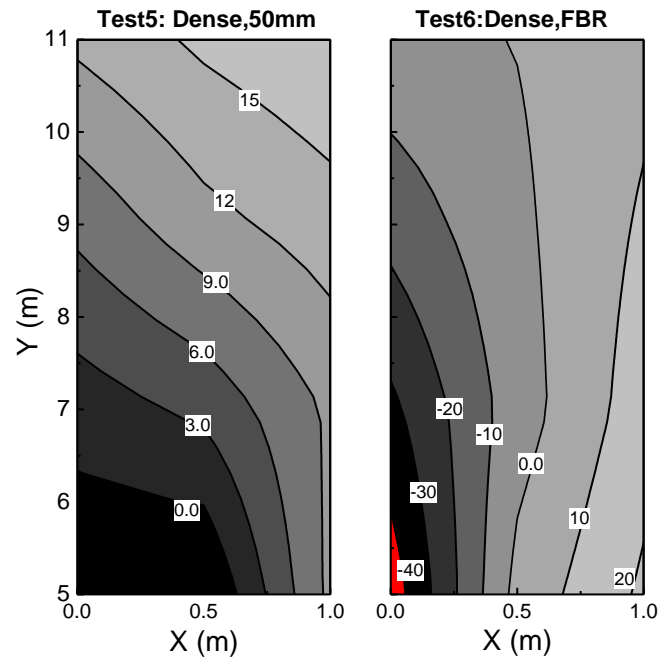
Fig. 14 Temperature distribution area of the dense CO_2 release experiments with three different orifices (15 mm, 50 mm and FBR).
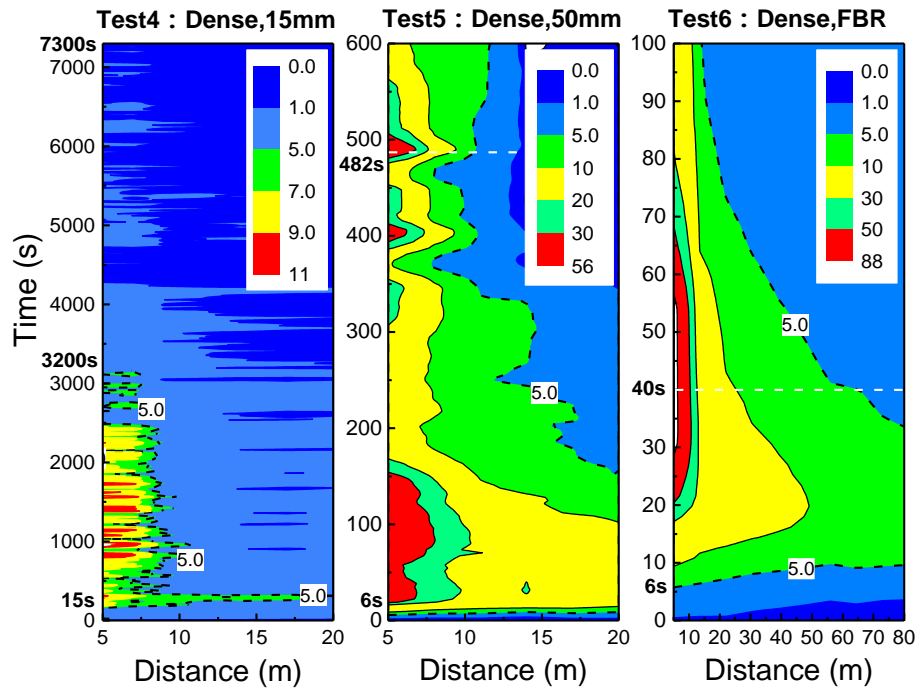
Fig. 15 CO_2 concentration development along the centerline of the dense CO_2 release experiments with three different orifices (15 mm, 50 mm and FBR).